Electronic and dynamic studies of boron carbide nanowires

D. N. McIlroy, Daqing Zhang, Robert M. Cohen, and J. Wharton

Department of Physics and Microelectronics Research and Communications Institute, Engineering and Physics Building,
University of Idaho, Moscow, Idaho 83844-0903

Yongjun Geng and M. Grant Norton

School of Mechanical and Materials Engineering, Washington State University, Pullman, Washington 99164-2920

Gelsomina De Stasió

Institut de Physique Appliquée, Ecole Polytechnique Fédérale, CH-1015 Lausanne, Switzerland
and Istituto di Struttura della Materia del CNR, Via Fosso del Cavaliere, I-00137 Roma, Italy

B. Gilbert and L. Perfetti

Institut de Physique Appliquée, Ecole Polytechnique Fédérale, CH-1015 Lausanne, Switzerland

J. H. Streiff, B. Broocks, and Jeanne L. McHale

Department of Chemistry, Renfrew Hall, University of Idaho, Moscow, Idaho 83844-2343

The electronic and vibrational properties of boron carbide nanowires grown by plasma-enhanced chemical vapor deposition have been examined with the techniques of near-edge x-ray absorption fine structure (NEXAFS) spectroscopy and Raman spectroscopy. The B $1s$ absorption edge is characterized by a narrow π^* resonance characteristic of sp/sp^2 hybridization followed by a broad σ^* resonance characteristic of sp^3 hybridization. The C $1s$ NEXAFS spectrum is dominated by the σ^* resonance indicating that C bonding in the nanowires is predominantly sp^3 in character. The NEXAFS spectra are equivalent to corresponding spectra of single-crystal (B_4C) boron carbide, consistent with the B_4C structure of the nanowires as determined by selected area electron diffraction. Four corresponding Raman modes of crystalline boron carbide have been observed for the boron carbide nanowires. Two previously unobserved Raman modes of boron carbide at 1365 and 1965 cm^{-1} have also been observed, which are specific to boron carbide nanowires. [S0163-1829(99)10231-5]

I. INTRODUCTION

Over the past decade significant effort has gone into developing an understanding of quantum confinement and its effects on electronic transport. This has been driven by scientific curiosity, as well as the need to quantify the role quantum confinement plays in microprocessor performance as the architecture of these devices heads towards the nanometer regime. Nanometer sized materials can be artificially manufactured, as well grown in a self-assembled fashion via novel processes. One of the advantages of exploring the properties of self-assembled nanostructures is their ease of construction. Self-assembled nanostructures come in a variety of flavors ranging from free standing nanocrystals grown by colloidal chemistry[1,2] to carbon nanotubes,[3] to name a few, and like multilayer quantum well systems they have been found to exhibit quantum size effects.[4,5]

In order to develop a full understanding of quantum size effects in self-assembled nanostructured materials a detailed understanding of their fundamental properties needs to be determined. Due to their large surface area to volume ratio, the fundamental properties of all types of nanostructured materials can be anticipated to deviate from those of the bulk. In addition, the surfaces of nanostructured materials can vary significantly with size, which will inevitably affect their elec-tronic properties. An excellent example of this phenomena was illustrated with carbon nanotubes where it was shown that changes in their structure altered their electronic properties from graphitic to semiconducting in character.[6] This work, as well as studies of semiconducting nanoparticles,[5] also demonstrated the feasibility of constructing nanoscale devices using self-assembled nanostructures. The work with carbon nanotubes has demonstrated the need to explore the structural properties of nanostructured materials, as well as stressed the need to examine their fundamental properties in order to develop a global understanding of their electronic transport properties relative to the bulk. In addition to quantum confinement, finite size effects can have a significant impact on the thermodynamic properties and vibrational density of states of nanostructured materials. Consequently, it is important that finite size effects be thoroughly explored in order to gauge the different factors that influence the properties of nanostructured materials.

In this paper, we have examined the electronic and vibrational structure of single-crystal boron carbide (B_4C) nanowires by near-edge x-ray absorption fine structure (NEXAFS) and Raman spectroscopy, respectively. Boron carbide is a refractory semiconductor material, which in addition to being chemically robust, has a very high-melting temperature in excess of 2400 °C. The mechanical hardness and elec-

tronic properties of single-crystal and amorphous boron carbide make it an attractive material for high temperature applications in materials[7–9] and electronics.[10–12] The crystal structure of boron carbide is rhombohedral (hR 15; S.G. R3m) and consists of 12-atom icosahedral units located at the corners of a rhombohedral unit cell connected by C-B-B or C-B-C chains lying along the cell diagonal.[13–20] This unique structure may lead to novel quantum transport effects at reduced dimensions. These studies will assist in the evaluation of the electronic and vibrational properties of boron carbide nanowires as they compare to bulk boron carbide.

II. SAMPLE PREPARATION

The nanowires were grown on (100)-oriented silicon substrates. Prior to insertion into the chamber the Si substrates were cleaned for 5 min in a 5% hydrofluoric acid/deionized water solution followed by a rinse in deionized water. The boron carbide nanowires were grown in a custom parallel plate 13.56-MHz plasma-enhanced chemical-vapor deposition (PECVD) chamber, which has been discussed in more detail elsewhere.[21] The substrates were located on the grounded electrode during deposition. The deposition temperature was typically in the range 1100–1200 °C and the plasma power was 50 W. The source compound was *closo*-1, 2-dicarbadodecaborane ($C_2B_{10}H_{12}$), which will be referred to from here on as orthocarborane. Argon was used as the carrier gas and was allowed to flow through the source bottle that was held at a temperature of 50 °C during deposition. The gas mixture consisted of 65 mTorr of Ar (10 sccm) and 25 mTorr of orthocarborane/Ar (3.5 sccm). A mat of boron carbide nanowires approximately 1 μm in thickness was obtained after two hours of deposition using the aforementioned experimental conditions.

III. EXPERIMENTAL DETAILS

The structural properties of the boron carbide nanowires were examined using an Amray 1830 scanning electron microscope (SEM) operated at 10–20 kV and a Philips CM200 analytical transmission electron microscope (TEM) operated at 200 kV. NEXAFS spectra where acquired using the imaging photoelectron spectromicroscope MEPHISTO,[22] which was attached to the 10-m TGM beamline at the Synchrotron Radiation Center in Stoughton, WI. Briefly, monochromatic soft x-rays are incident on the sample at 60° off the surface normal with the photoelectrons collected over a 2π sterad spherical angle. The B 1s NEXAFS spectra were normalized to the photon flux, while the C 1s spectra were normalized to a NEXAFS spectrum acquired across the C 1s absorption edge obtained from a carbon-free Si surface. This normalization procedure eliminates spurious structure from being introduced into the C 1s spectra by carbon contamination on the beamline optics. The surfaces of the samples were found to be relatively free of oxygen upon examination of the intensity of the C 1s absorption edge. The fundamental mode of operation of the microscope is photoelectron emission by x-ray excitation. Raman spectra were excited at a wavelength of 457 nm using an argon ion laser. The Raman

(a)

(b)
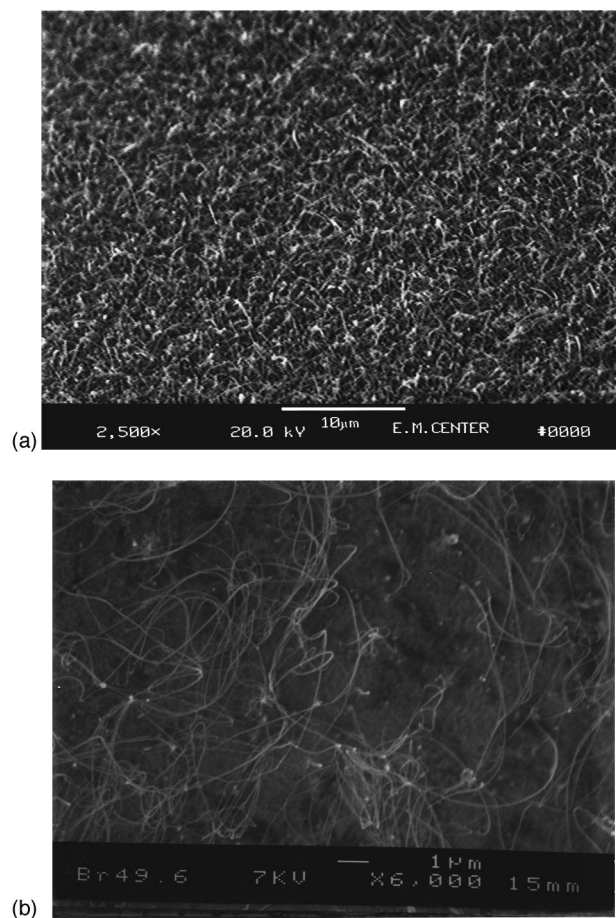
FIG. 1. (a) SEM image of a high-density mesh of boron carbide nanowires, (b) a SEM image of a low-density boron carbide nanowire film.

spectra were acquired in a specular geometry at a beam incidence angle of 45°. The scattered light was dispersed and analyzed using a double monochromator.

IV. NANOWIRE STRUCTURE

The boron carbide nanowires grow by a vapor-liquid-solid mechanism, which is described in detail elsewhere.[23] A typical example of a boron carbide nanowire thin film grown on Si is displayed in Fig. 1(a), which shows that the film consists of a mesh of boron carbide nanowires. Figure 1(b) is an SEM image of a low density mat, which gives a clear picture of the high aspect ratio of the nanowires. A closer inspection of the film with a TEM (Fig. 2) reveals the presence of smooth walled nanowires and indicates that the wires grow in a range of diameters from 10 nm up to 75 nm. Some rough walled nanowires and rhombohedral nanocrystals connected by nanowires (necklaces), which are not shown in Fig. 2, have also been observed.[23] Nanowires make up 90% of the film, with the other 10% consisting of rough walled wires and necklace structures. Selected-area diffraction of the nanowires and the rhomboidal structures indicate that both structures are monocrystalline with a rhombohedral crystal structure (hR15; S.G. R3m).[23] Due to the identical crystal structures and similar lattice parameters of $B_{13}C_2$ (a = 0.5617, b = 0.5617, c = 1.2099 nm) and B_4C (a = 0.5600,
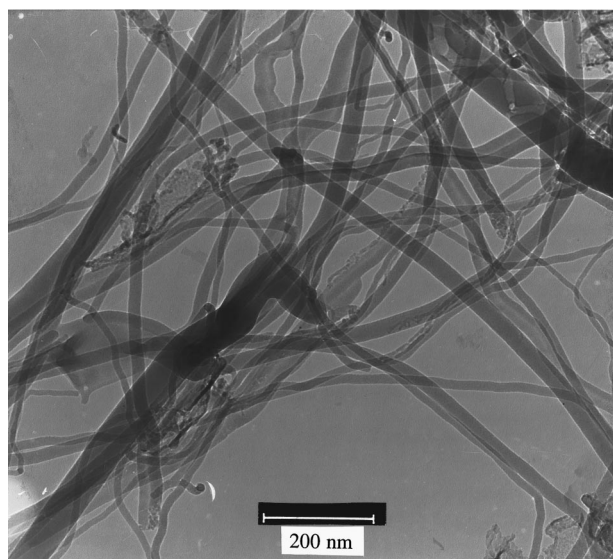
FIG. 2. A bright field TEM image of boron carbide nanowires grown by PECVD.

$b = 0.5600$, $c = 1.2086$ nm) it is not possible to unambiguously identify with electron diffraction which boron carbide phase is present. Energy dispersive spectroscopy (EDS) measurements performed at a variety of locations on individual nanowires indicate that the B:C ratio is close to 4:1, which indicates that the nanowires are single-crystal B_4C rather than $B_{13}C_2$. The EDS measurements were made using a focused electron probe that was positioned at various places along each nanowire. The x-ray spectrum was recorded for each location and the B:C ratios determined from the relevant integrated peak intensities.
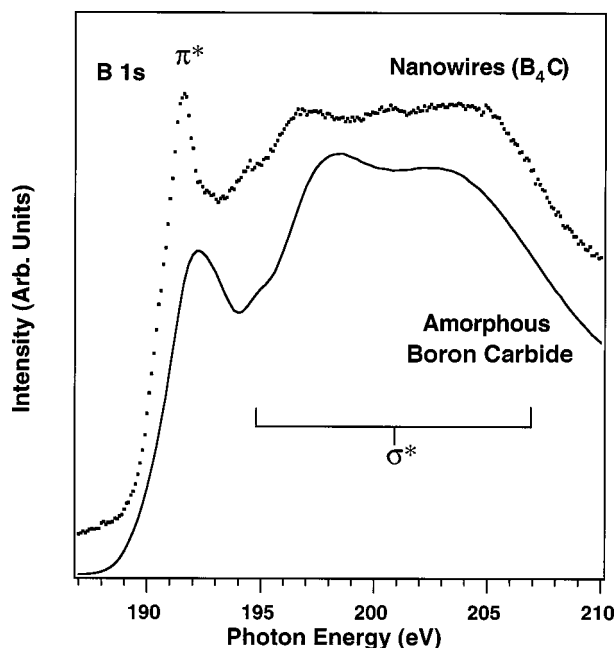
FIG. 3. NEXAFS spectra across the B $1s$ absorption edge of a boron carbide nanowire film (●) and an amorphouslike boron carbon alloy (solid line).
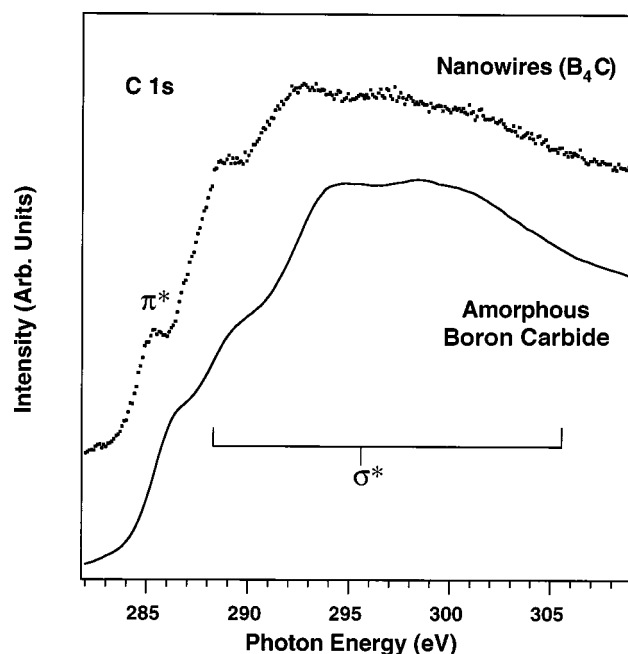
FIG. 4. NEXAFS spectra across the C $1s$ absorption edge of a boron carbide nanowire film (●) and an amorphouslike boron carbon alloy (solid line).

V. EXPERIMENTAL RESULTS

In Figs. 3 and 4 we present NEXAFS spectra of the B $1s$ and C $1s$ absorption edges, respectively, acquired from the boron carbide nanowire film shown in Fig. 1. The B $1s$ absorption edge is characterized by an onset of a sharp antibonding π^* state at 190 eV and σ^* states from 196 to 208 eV. The π^* and σ^* assignments are based on comparisons to single crystal boron carbide[24] and hexagonal boron nitride.[25,26] The full width at half maximum of the B $1s$ π^* resonance in Fig. 3 ($\sim$1 eV) is consistent with NEXAFS spectra acquired from polycrystalline B_4C.[24]

The C $1s$ NEXAFS spectrum in Fig. 4 for the C $1s$ edge is characterized by a weak π^* state resonance at 285.5 eV and broad σ^* states which onset at 287.5 eV and extend beyond 300 eV. These assignments are consistent with previous studies of B_4C by Jiménez *et al.*[24] This earlier study of polycrystalline boron carbide[24] observed a higher level of fine structure in the C $1s$ NEXAFS spectrum than in this study, which we attribute to the higher resolution of the monochromator used in that study.
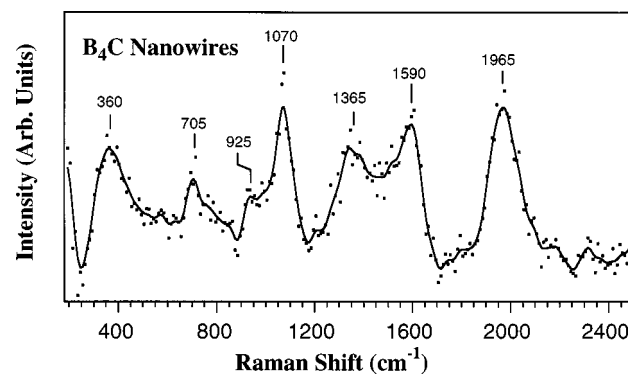
FIG. 5. Background corrected Raman spectrum of a boron carbide nanowire film excited a wavelength of 457 nm.

TABLE I. Raman modes of boron carbide.

	Peak position (cm^{-1})		
B_4C Nanowires	$^{15}B_{4.3}C$ (single crystal)	$^{18}B_{4.3}C$ (polycrystalline)	^{15}Symmetry
*	270	275	A_{1g}
360	320	326	A_{1g}
*	420	430	A_{1g}
*	449		E_g
	477	489	E_g
	532	551	E_g
	560	599	E_g
	591	637	E_g
	652	671	E_g
705	725	748	E_g
*	797	821	A_{1g}
*	869	895	A_{1g}
925	928	958	A_{1g}
*	990	1009	
1070	1065	1108	A_{1g}
1365			
1590	1590	1598	
1965			

*Appear as shoulders in the spectrum.

In Fig. 5 we present a Raman spectrum obtained from the sample shown in Fig. 1. The spectrum is dominated primarily by B_4C modes based on comparisons with Raman studies of single-crystal boron carbide.[15,18,27] These modes are at 360, 705, 925, 1070, and 1590 cm^{-1}. The mode at 2175 cm^{-1} is attributed to a second-order excitation of the line at 1070 cm^{-1} ($\sim 2 \times 1070$ cm^{-1}) and the line at 2315 cm^{-1} is likely due to a combination of the second-order excitation of the line at 360 cm^{-1} and the line at 1590 cm^{-1} ($\sim 2 \times 360 + 1590$ cm^{-1}). Previously unobserved Raman modes of B_4C are observed at 1345 and 1975 cm^{-1} in Fig. 5.

VI. DISCUSSION

A. NEXAFS spectroscopy of boron carbide nanowires

The sharpness of the B 1s π^* resonance can be used as a relative measure of the degree of short-range order of boron carbide materials. In Fig. 3, a NEXAFS spectrum of an amorphouslike boron-carbon (a-BC) alloy film grown by PECVD has been included to illustrate the broadening of the π^* resonance, which occurs with increasing disorder. Upon comparison of the two spectra in Fig. 3 it is obvious that the degree of local order in the boron carbide nanowires is excellent. An increase in disorder diminishes the degree of fine structure in the σ^* region of the B 1s absorption in Fig. 3. The intensity of the B π^* state relative to the σ^* states gives a qualitative measure of ratio of sp/sp^2 hybridization to sp^3 hybridization. A comparison of the two spectra in Fig. 3 indicates that disorder is accompanied by a reduction in sp/sp^2 bonding of boron. Jiménez et al.[24] observed similar effects in annealing experiments of boron carbide where it was observed that C segregation occurred at an annealing temperature of 1900 °C. This was accompanied by a corresponding decrease in the B π^* resonance.

Examination of the C 1s NEXAFS spectra of the boron carbide nanowires and the a-BC film in Fig. 4 shows similar broadening effects with increased disorder. The intensity of the C π^* state relative to the σ^* states gives a qualitative measure of ratio of sp/sp^2 hybridization to sp^3 hybridization and indicates that C bonding is predominantly sp^3 in character. Due to the inequivalence of the C bonding sites, sp^3 character is attributed to C atoms occupying CBC or CBB chains and sp^2 character to C atoms located in sites within the icosahedral structures.[24] The boron carbide nanowire C 1s NEXAFS in Fig. 4 is qualitatively similar to NEXAFS studies of polycrystalline boron carbide by Jiménez et al.,[24] with the exception of more detailed fine structure in the region of the π^* resonance. Again, this is attributed to the higher resolution of their experimental setup.

B. Raman spectroscopy of boron carbide nanowires

The Raman modes of the boron carbides wires are summarized in Table I. Also included in Table I are the Raman modes of polycrystalline[15] and single-crystal[18] boron carbide. Due to finite size effects which can broaden Raman spectral features,[28] we were unable to resolve all of the Raman modes of polycrystalline[15] and single-crystal[18] boron carbide. However, the dominant Raman modes of polycrystalline and single-crystal boron carbide are observed in the nanowire spectrum in Fig. 5 at 360, 705, 925, 1070, and 1590 cm^{-1}. Examination of Fig. 5 reveals that the majority of the unresolved modes of boron carbide can be accounted for in the broad shoulders of the primary Raman modes of the nanowires.

Also included in Table I are the symmetry assignments of the Raman-allowed modes. These assignments have been determined from group theory[29] based on the D_{3d} symmetry of

idealized boron carbide and yield 11 Raman-active modes, $5A_{1g}$ and $6E_g$. Based on the assignments of Ref. 20, the modes centered around 360 and 925 cm^{-1} can be attributed to A_{1g}-type fundamental modes of equatorial pentagons of three icosahedra as opposed to the assignment of these modes to C-B-C chain structures.[18] Examination of Fig. 1(b) reveals that many of the boron carbide nanowires bend back on themselves and suggests that they are under significant strain. The boron carbide nanowire Raman mode centered on 360 cm^{-1} is shifted upward in energy by approximately 40 cm^{-1} relative to the corresponding modes of polycrystalline and single crystal boron carbide in Table I. This upward shift may be a strain induced effect that shifts the vibrational modes to higher wave numbers, as opposed to finite size effects that typically shift Raman modes downward.[28] If the modes at 360 and 925 cm^{-1} are either exclusively chain modes or intericosahedral modes, we would anticipate that they would exhibit similar shifts. Note that the nanowire Raman mode at 925 cm^{-1} is in excellent agreement with the corresponding mode of polycrystalline boron carbide. Consequently, we suggest that one of these modes is associated with chain modes and the other with intericosahedral modes. By accounting for strain in theoretical models of the vibrational density of states of the boron carbide nanowires it should be possible to resolve this issue.

The modes at 705 and 1070 cm^{-1} have a symmetry assignment of A_{1g} and are attributed either to icosahedral breathing modes[18] or two-center B-B vibrations between covalently bonded polar atoms of neighboring icosahedra.[15] The mode at 1590 cm^{-1} has been attributed to C-B-B chain modes.[15] The previously unobserved mode at 1365 cm^{-1} has a number of possible origins. The first is that this mode and the mode at 1590 cm^{-1} are signatures of amorphous carbon. While double peaks at 1365 and 1590 cm^{-1} have been observed for amorphous carbon, they have been attributed to the presence of microcrystalline graphitic carbon.[30,31] Similar Raman peaks have been observed for films of aligned carbon nanotubes,[32] yet high-resolution TEM measurements of the nanotube samples found no evidence for microcrystalline graphitic carbon. These modes instead have been attributed to defects in the carbon nanotubes. Electron diffraction patterns recorded for these boron carbide nanowire samples showed no evidence of the broad diffusion rings typical of amorphous carbon. TEM analysis of the boron carbide nanowire films exclude the presence of amorphous carbon or microcrystalline graphitic carbon. Furthermore, it has been demonstrated that amorphous and graphitic carbon have very distinct signatures in NEXAFS spectra across the C 1s edge.[24] These studies by Jiménez *et al.*[24] showed that the signatures of amorphous carbon or graphitic carbon in C 1s NEXAFS spectra of boron carbide are an extremely sharp π^* resonance in conjunction with a sharp onset of the σ^* states, where the intensity of the π^* resonance is significantly larger than that of the σ^* states. The lack of these signatures of amorphous or graphitic carbon in the C 1s NEXAFS spectrum of the boron carbide nanowires in Fig. 4 further supports the conclusion that neither of these phases of carbon are present in the samples used in this study. It is also worth noting that the VLS growth mechanism procludes the inclusion of amorphous or graphitic carbon into the nanowires. Consequently, we attribute the mode at 1365 cm^{-1} to a Ra-

man active mode specific to the boron carbide nanowires. Due to the unique curvature of the surface of the nanowires, as well as the large surface area to volume ratio, we suggest that the Raman mode at 1365 cm^{-1} originates from surface terminations unique to the nanowires. A detailed understanding of the surface structure of these nanowires, as well as calculations of the Raman active modes, will need to be performed in order to accurately determine the origin of the mode at 1365 cm^{-1}, as well as to conclusively demonstrate that it originates from the boron carbide nanowires rather than pockets of amorphous or graphitic carbon.

In addition to the mode at 1365 cm^{-1}, a strong mode at 1965 cm^{-1} is observed in the Raman spectrum in Fig. 5. This mode could originate from a combination of the modes at 270 and 1590 cm^{-1}, although the intensity of the mode at 1965 cm^{-1} relative to the aforementioned modes would tend to preclude this assignment. In addition, no corresponding modes at this wave number have been observed for bulk samples of boron carbide[15,18] or microcrystalline graphitic carbon.[30,31] Consequently, we have concluded that this mode is also specific to boron carbide nanowires. Until detailed calculations of the vibrational properties of these boron carbide nanowires can be performed, the origin of the modes at 1365 and 1965 cm^{-1} can only be speculated. Some potential assignments are that these modes arise from collective excitations of the nanowires in the form of transverse, longitudinal, or breathing modes. Assignments of these types have been made for carbon nanotubes.[33] While we are not suggesting that the boron carbide nanowire modes at 1365 and 1965 cm^{-1} are equivalent to those carbon nanotubes, we do suggest similar modes of these type should be Raman active for boron carbide nanowires.

Finally, given the small diameter of the nanowires ($\sim$25 nm), we would anticipate that finite size effects will be significant. Yet with the exception of the modes at 360 and 705 cm^{-1}, there are no apparent shifts of the Raman modes of the nanowires relative to the bulk modes of boron carbide, which suggests that the influences of finite size effects are minimal. This is surprising since theoretical calculations of metallic nanocrystals[34] indicate that finite size effects will have a significant impact on the vibrational density of states. However, due to the complicated crystal structure of boron carbide, finite size effects may manifest themselves in ways unique to this system. Given the lack of obvious finite size effects, these results suggest that the thermodynamic properties of the boron carbide nanowires will be equivalent to those of bulk boron carbide. Again, these results may be expected given the unique structure of boron carbide. Further experimental and theoretical studies will need to be conducted in order to resolve this issue.

VII. CONCLUSIONS

The electronic structure of boron carbide nanowires, as determined with NEXAFS spectroscopy, is very similar to that of bulk boron carbide. The onset of the B 1s absorption edge of the nanowires is dominated by a strong π^* resonance, which is expected for well-ordered boron carbide. The C 1s edge is predominantly sp^3 in character and is consistent with bulk boron carbide. These results are also consistent with structural studies that indicate that the composition of

these nanowires is B_4C, the most stable form of boron carbide. The predominant sp^3 character of these nanowires further suggests that they are extremely hard and should have excellent mechanical properties. Congruent with the NEXAFS measurements, the Raman spectrum of the nanowires is equivalent to that of single-crystal and polycrystalline boron carbide, with the exception of two previously unobserved modes at 1365 and 1965 cm^{-1}. TEM studies rule out the presence of graphitic or amorphous carbon and therefore it has been concluded that these two modes are a consequence of the novel shape and size of the boron carbide nanowires. Furthermore, we have suggested that they arise from transverse, longitudinal, and or breathing modes of the nanowires. These initial Raman studies tend to preclude the influence of finite size effects as they pertain to the vibrational density of states.

[1] L. Brus, Appl. Phys. A: Solids Surf. **53**, 465 (1991).

[2] A. P. Alivisatos, Science **271**, 933 (1996).

[3] S. Iijima, Nature (London) **354**, 56 (1991).

[4] S. J. Tans, M. H. Devoret, H. Dai, A. Thess, R. E. Smalley, L. J. Geerligs, and C. Dekker, Nature (London) **386**, 474 (1997).

[5] D. L. Klein, R. Roth, A. K. L. Lim, A. P. Alivisatos, and P. L. McEuen, Nature (London) **389**, 699 (1997).

[6] P. G. Collins, A. Zettl, H. Bando, A. Thess, and R. E. Smalley, Science **278**, 100 (1997).

[7] A. J. Pyzik and D. R. Beaman, J. Am. Ceram. Soc. **78**, 305 (1995).

[8] L. L. Wang, Z. A. Munir, and J. B. Holt, J. Am. Ceram. Soc. **78**, 756 (1995).

[9] L. S. Sigl and H. J. Kleebe, J. Am. Ceram. Soc. **78**, 2374 (1995).

[10] S.-D. Hwang, N. B. Remmes, P. A. Dowben, and D. N. McIlroy, J. Vac. Sci. Technol. B **14**, 2957 (1996).

[11] S.-D. Hwang, P. A. Dowben, Ahmad A. Ahmad, N. J. Ianno, J. Z. Li, J. Y. Lin, H. X. Jiang, and D. N. McIlroy, Appl. Phys. Lett. **70**, 1028 (1997).

[12] D. N. McIlroy, S.-D. Hwang, Ken Yang, N. Remmes, P. A. Dowben, Ahmad A. Ahmad, N. J. Ianno, J. Z. Li, J. Y. Lin, and H. X. Jiang, Appl. Phys. A: Mater. Sci. Process. **69**, 335 (1998).

[13] Charles Wood and David Emin, Phys. Rev. B **29**, 4582 (1984).

[14] I. A. Howard and C. L. Beckel, Phys. Rev. B **35**, 2929 (1987).

[15] D. R. Tallant, T. L. Aselage, A. N. Campbell, and D. Emin, Phys. Rev. B **40**, 5649 (1989).

[16] U. Kuhlmann and H. Werheit, Solid State Commun. **83**, 849 (1992).

[17] U. Kuhlmann, H. Werheit, and K. A. Schwetz, J. Alloys Compd. **189**, 249 (1992).

[18] U. Kuhlmann and H. Weheit, J. Alloys Compd. **205**, 87 (1994).

[19] M. Carrad and D. Emin, Phys. Rev. B **51**, 11 270 (1995).

[20] B. Morosin, G. H. Kwei, A. C. Lawson, T. L. Aselage, and D. Emin, J. Alloys Compd. **226**, 121 (1995).

[21] S. Lee, J. Mazurowski, G. Ramseyer, and P. A. Dowben, J. Appl. Phys. **72**, 4925 (1992).

[22] Gelsomina De Stasio, M. Capozi, G. F. Lorusso, P. A. Baudat, T. C. Droubay, P. Perfetti, G. Margaritondo, and B. P. Tonner, Rev. Sci. Instrum. **69**, 2062 (1998).

[23] Daqing Zhang, D. N. McIlroy, Yongjun Geng, and M. Grant Norton (unpublished).

[24] I. Jiménez, D. G. J. Sutherland, A. van Buuren, J. A. Carlisle, L. J. Terminello, and F. J. Himpsel, Phys. Rev. B (to be published).

[25] I. Jiménez, A. Jankowski, L. J. Terminello, J. A. Carlisle, D. G. J. Sutherland, G. L. Doll, J. V. Mantese, W. M. Tong, D. K. Shuh, and F. J. Himpsel, Appl. Phys. Lett. **68**, 2816 (1996).

[26] I. Jiménez, A. Jankowski, L. J. Terminello, D. G. J. Sutherland, J. A. Carlisle, G. L. Doll, W. M. Tong, D. K. Shuh, and F. J. Himpsel, Phys. Rev. B **55**, 12 025 (1997).

[27] H. Werheit, in *The Physics and Chemistry of Carbides; Nitrides and Borides*, edited by R. Freer (Kluwer, Netherlands, 1990), pp. 705–725.

[28] T. Werninghaus, J. Hahn, F. Richter, and D. R. T. Zahn, Appl. Phys. Lett. **70**, 958 (1997).

[29] H. Binnenbruck and H. Werheit, Z. Naturforsch., A: Phys. Sci. **42**, 787 (1979).

[30] J. Schwan, S. Ulrich, V. Batori, H. Ehrhardt, and S. R. P. Silva, J. Appl. Phys. **80**, 440 (1996).

[31] M. A. Tamor and W. C. Vassell, J. Appl. Phys. **76**, 3823 (1994).

[32] W. Li, H. Zhang, C. Wang, Y. Zhang, L. Xu, K. Zhu, and S. Xie, Appl. Phys. Lett. **70**, 2684 (1997).

[33] A. M. Rao, E. Richter, S. Bandow, B. Chase, P. C. Eklund, K. A. Williams, S. Fang, K. R. Subbaswamy, M. Menon, A. Thess, R. E. Smalley, G. Dresselhaus, and M. S. Dresselhaus, Science **275**, 187 (1997).

[34] A. Kara and T. S. Rahman, Phys. Rev. Lett. **81**, 1453 (1998).